Laser Diagnostic Investigation of the Bubble Eruption Patterns in the Freeboard of Fluidized Beds: Simultaneous Acetone PLIF and Stereoscopic PIV Measurements

C. R. Müller, G. Hartung, J. Hult, and J. S. Dennis
Dept. of Chemical Engineering, Pembroke Street, University of Cambridge, Cambridge, CB2 3RA, U.K.

C. F. Kaminski
Dept. of Chemical Engineering, Pembroke Street, University of Cambridge, Cambridge, CB2 3RA, U.K., and
Institute of Optics, Information and Photonics, University of Erlangen-Nuremberg, Günther-Scharowsky-Str. 1,
91058 Erlangen, Germany

DOI 10.1002/aic.11802
Published online April 20, 2009 in Wiley InterScience (www.interscience.wiley.com).

For the first time PIV has been applied simultaneously with acetone-PLIF in the freeboard of a fluidized bed. Here, the eruption profile of single bubbles and a continuous stream of bubbles were studied. As stereoscopic PIV was applied the out-of-plane component of the velocity was also measured. The out-of-plane component is not negligible. The observed bubble eruption patterns were in general agreement with the bubble model of Levy and Lockwood,[24] Yorquez-Ramirez and Duursma[5] and Solimene et al.[1] No qualitative difference between the eruption of a single bubble and a stream of bubbles was observed. Based on the calculated vorticity of the gas in the freeboard, it was found that the bubble induced turbulence decays fairly rapidly. © 2009 American Institute of Chemical Engineers *AIChE J*, 55: 1369–1382, 2009
Keywords: fluidized beds, PIV, PLIF, bubble eruption, freeboard

Introduction

An important problem where a fluidized bed is used as a combustor or gasifier is the segregation of bed material, including fuel particles particularly where these are from biomass or low-rank coal, to the top of the bed. Consequently, a significant amount of the carbon content of the fuel can be released in the form of volatiles directly into the freeboard. The volatile matter then reacts via homogeneous combustion in the freeboard with the air leaving the bed. The extent of gas mixing in the freeboard is important in determining the destruction and formation of pollutants, such as NO_x, and the rate of heat release by combustion.

Studies of the hydrodynamics of gas flow in the freeboard of gas-fluidized beds have mainly addressed the entrainment and elutriation of bed particles. Above the so-called transport disengaging height (TDH), the rate of entrainment and the size distribution of the entrained particles are fairly constant. However, due to the lack of appropriate experimental techniques, the detailed physics of the entrainment process, i.e., the very complex structure of the velocity field of the gas and the particles in the freeboard has not been studied. It is well accepted that the turbulence in the freeboard is induced by the eruption of bubbles at the surface. However, the actual interaction between the gas of an erupting bubble, the bed particles and the gas in the freeboard is only poorly understood.

Correspondence concerning this article should be addressed to C. R. Müller cm433@cam.ac.uk

The first studies of the measurement of the velocity profile of the gas in the freeboard used either hot wire anemometry[8] or laser doppler anemometry.[2,24] Both techniques are, however, only able to provide point measurements. Pemberton and Davidson[8] and Levy and Lockwood[24] observed very large, bubble-induced, velocity fluctuations in the freeboard, with the velocity fluctuations being of the same order of magnitude as the mean gas velocity.[8] Quite surprisingly, the maxima of the gas velocities were observed near the walls.[24] More recently, PIV has been applied to image the flow pattern in the freeboard above an erupting bubble.[7] Bubble-induced eddies were observed in the freeboard and, in agreement with Levy and Lockwood,[24] the maxima of the gas velocities were observed near the walls. The velocity in the center of the freeboard was, depending on vertical position in the freeboard, negative or close to zero.

Two early models were proposed to describe bubble eruption and subsequent disturbance of the freeboard: (1) the pulsed jet theory proposed by Zenz and Weil,[4] and (2) the ghost bubble theory of Kehoe[9] and Pemberton and Davidson.[8] The pulsed jet theory[4] postulates that bubbles erupting at the surface behave as intermittent jets. These jets give rise to a highly irregular profile of gas velocity across the column. With height, the velocity fluctuations gradually dissipate and equilibrate to the superficial gas velocity. The theory of ghost bubbles[8,9] is based on observations made of the eruption of bubbles at the top of a liquid fluidized bed. Here, it is assumed that, after eruption, the bubble retains its shape, forming a ''ghost bubble''. The ghost bubble decelerates, as surrounding fluid is entrained in the rear of the bubble.

Based on the experimental observation of a toroidal circulation, a different eruption model was proposed by Levy and Lockwood.[24] After the eruption of a bubble, the ejected bed particles reverse their flow direction and fall back into the bed. The drag force of these falling particles is then sufficient to cause a flow reversal in the surrounding gas. This downward motion creates a toroidal vortex, which initially expands toward the walls. This is followed by a vertical motion, carried upward by the main gas flow in the freeboard. Solimene et al.[1,3] and Yorquez-Ramirez and Duursma[5] proposed very similar models, but describing in more detail the release of the gas of the erupting bubble as it forms a dome. Solimene et al.[1,3] reported the formation of a ''nose pocket'' of gas, the size of which depends on the size of the fluidized particles comprising the dome. This pocket of gas is released at the center of the dome. On the other hand Yorquez-Ramirez and Duursma[5] proposed a rather evenly distributed release of gas along the dome upon bubble eruption.

Laser diagnostic imaging techniques are nonintrusive and are, for example, capable of providing information about, for example, concentration, temperature and velocity fields. Planar laser induced fluorescence (PLIF) is of interest in this context, as it permits highly sensitive concentration measurements of e.g., flame radicals or of tracers species seeded into a flow. In fluid mechanical applications, acetone-PLIF has been developed into a standard tool for mixture-fraction measurements.[10–13] Quantitative studies of mixing in flows that are isothermal and isobaric are straightforward, as a constant fluorescence yield can be assumed, which permits acetone number density to be considered directly proportional to the fluorescence signal. The freeboard of a fluidized bed, as investigated in this work, provides an environment of constant temperature and pressure. Even though acetone-PLIF has become a standard tool for applications in unreacting jets and combustion processes, challenges for its application in fluidized beds still remain.

Over the last decade particle image velocimetry (PIV) has developed into a standard laser diagnostic tool for exploring the velocity in both, the liquid and gas phase flows.[14–17] PIV is a technique which measures, the velocity of e.g., a stream of gas, by correlating the motion of a small ensemble of seeding particles between two successively acquired images. Using only a single CCD-camera, the out-of-plane dimension of the object field cannot be resolved. Instead, the out-of-plane component is projected on to the object plane causing a perspective error of the in-plane component as is illustrated in Figure 1. To overcome this error, Stereoscopic PIV (SPIV) can be used; this uses two cameras to record two simultaneous off-axis views of the same region of interest of the scattered light from the laser sheet. Sufficient information is contained in the two views both to extract the out-of-plane velocity component of particles V_z, and to eliminate the perspective error in the in-plane velocity components.

As shown schematically in Figure 1a, 2D-PIV only allows the projection of the velocity vector in the object plane to be inferred (V'_x and V'_y). In the case of constant magnification M the perspective error is directly proportional to the viewing angle subtended by the position of the particle relative to the axis of the camera. In contrast, stereoscopic PIV (Figure 1b) can eliminate the projection error, yielding accurate measurements of all three components of the velocity (V_x, V_y and V_z). The SPIV-method depicted in Figure 1b is referred to as the rotational method, as the two camera axes are rotated around the vertical axis, such that the central rays of the camera lenses intersect the object plane at the system axis. A disadvantage with this approach is that the magnification over the field of view is no longer uniform. In addition, as shown in Figure 1b, the image plane has to be rotated with respect to the lens plane by an angle θ such that the object plane, lens plane and image plane are collinear. This requirement is referred to as the Scheimpflug condition. It guarantees that all areas of the object plane are in good focus on the image plane. Yoon and Lee[26] reported a direct comparison between 2D-PIV and SPIV setups. Their study showed that the difference between the mean in-plane velocity components, measured by 2D-PIV and SPIV techniques, is nearly proportional to the mean out-of-plane velocity component.

This work is a significant extension of the work of Solimene et al.[1] and Hartung et al.[19] as PLIF and PIV are applied simultaneously. This is intended to shed light onto the complex interactions taking place between erupting bubbles and the velocity profile of the gas in the freeboard. Optimization procedures for PLIF measurements, as reported in Hartung et al.[19] have been applied yielding excellent signal to noise (s/n)-ratio. This high (s/n)-ratio is crucial if particle image velocimetry (PIV) is applied simultaneously with acetone PLIF, as the seeding particles of PIV cause a significant reduction in visibility through the glass windows, resulting in a decreased acetone signal recorded by the ICCD

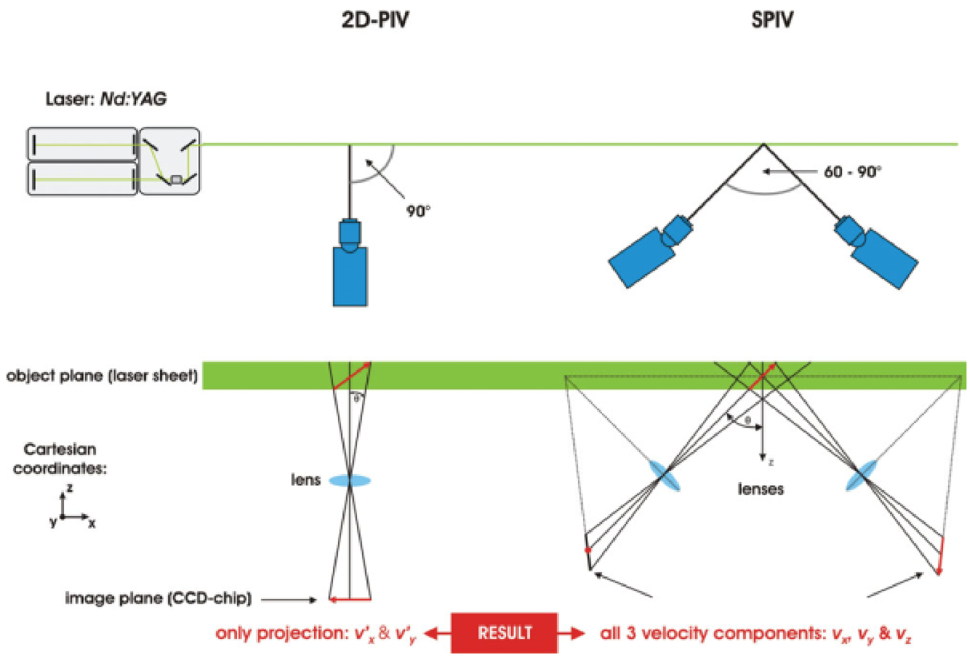

Figure 1. Comparison of 2-D-PIV and SPIV (rotational system). In 2D-PIV the velocity components are biased by the ratio of the out-of-plane velocity component to the in-plane velocity component and are, thus, referred to as V_x' and V_y' here.

[Color figure can be viewed in the online issue, which is available at www.interscience.wiley.com.]

camera. However, a disadvantage of the simultaneous PIV and PLIF acquisition compared with the PLIF acquisition alone is the reduced acquisition frequency, due to the software and hardware used in this study. Therefore, faster PLIF images acquired with a frequency of 5 Hz as reported in Hartung et al.[19] are used in conjunction with our new simultaneous PIV and PLIF measurements (acquisition frequency 2 Hz) to investigate the rather complex dynamics of bubble eruption. Beside the development of several opimisation measures the main conclusions of Hartung et al.[19] were:

1. Experimental measurements support the bubble eruption model of Levy and Lockwood,[24] Yorquez-Ramarez and Duursma[5] and Solimene et al.[1,3] and

2. Five different release pattern of gas at the moment of bubble eruption were identified.

This article is structured as follows. First, a detailed description of the laser diagnostics and the setup of the fluidized bed is given. This is followed by a presentation of the simultaneously acquired PIV and acetone-PLIF measurements. The results are discussed in the context of turbulence in the freeboard introduced by bubble eruption, and the main conclusions are summarized.

Experimental Setup

Fluidized bed and particles

The fluidized bed was of a square cross-section of a side-length of 200 mm, and made of steel. A schematic diagram is depicted in Figure 2a. The distributor consisted of a perforated aluminum plate of 1.5 mm thickness, containing 81 holes, each of 0.5 mm dia. oriented in a square array. This gave even fluidization, as the pressure drop over the distributor plate was larger than the weight of the bed at minimum fluidization. The air to fluidize the bed particles, glass ballotini sieved to size 150 – 250 μm, was fed into the fluidized bed via a windbox, 150 mm in height. To inject single bubbles, or a stream of bubbles, into an incipiently fluidized bed, a nozzle of 10 mm i.d. and 14 mm o.d. was mounted in the center of the distributor plate. To release single bubbles, a controlled volume of gas was injected into the bed via a pressure vessel and a solenoid valve; the pressure in the

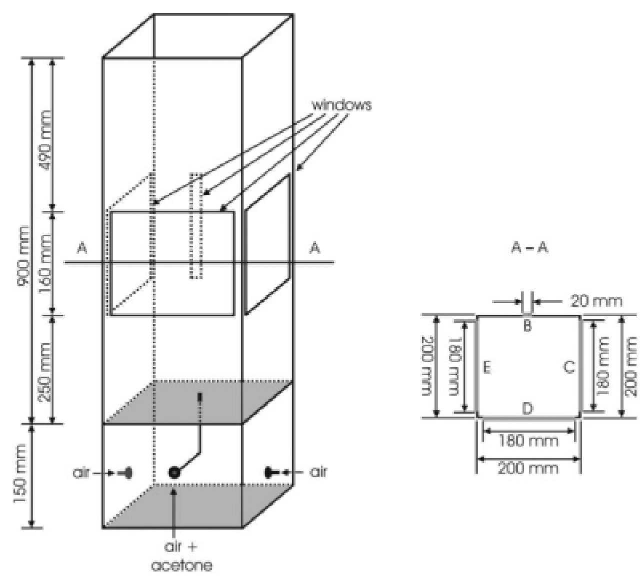

Figure 2. Schematic diagram of the fluidized bed used in this study.

vessel and the opening time of the valve could be varied. The overall height of the column containing the fluidized bed was 900 mm. The laser light accessed the splash-zone and freeboard of the fluidized bed through glass sheets mounted at a height of 250 mm; the arrangement is shown in Figure 2b. The Nd:YAG laser for PLIF entered via the 180 × 150 mm glass window (labeled "B" in Figure 2), whereas the two Nd:YAG lasers for PIV enter via the 180 × 160 mm glass window (labeled "D" in Figure 2). The ICCD camera imaging the fluorescence signal of the acetone receives light from the fluidized bed via the 180 × 160 mm glass window, labeled "E" in Figure 2b and the two ICCD cameras for PIV via the 180 × 160 mm glass window, labeled "C". The bed height at incipient fluidization was 250 mm, resulting in a bed aspect ratio of 1.25, typical for, e.g., a fluidized-bed gasifier. Particles (Sphericels hollow glass spheres type 110P8, mean dia. 11 μm, Potters Industries, U.K.) were seeded with a cyclone aerosol seeder (CAS) into the fluidized bed. The seeder design was adopted from.[25] A powder is suspended in the seeder, and the aerosol is drawn from the top. This design prevents large agglomerates leaving the seeder.

Laser diagnostics

1. PIV. 2D-PIV and SPIV measurements were performed to characterize the velocity fields in the freeboard above the fluidized bed. The experimental setup is depicted in Figure 3. The second harmonic from two frequency doubled pulsed Nd:YAG lasers (Continuum Surelite II, 35 mJ/pulse) was used to create an overlapping light-sheet of 620 μm thickness (FWHM). For SPIV, both cameras (Sensicam, PCO imaging, Germany, 1,280 × 1,024 pixels, double-frame mode) were arranged at 45° to each other as shown in Figure 3, with the lenses arranged according to the Scheimpflug criterion. For 2D-PIV, one camera (PIV A) was employed and arranged at 90° with respect to the laser sheet. Each camera was fitted with a narrow bandpass interference filter (centered at 532 nm, with 10 nm FWHM; peak transmission = 90 %) to reject ambient light. The separation between the PIV laser pulses was adjusted to match the flow rates, and varied from 5 ms to 8 ms. The PIV laser sheets were aligned through the center of the fluidized bed, as shown in Figure 3.

Davis 7.1 processing software (Lavision, Germany) was used to calculate velocity fields from the recorded data. After subtracting the minimum intensity level in each double frame image, the data were cross-correlated over successively smaller interrogation areas leading to a discrete window offset.[18] After each interrogation the peak-ratio in the cross correlation plane (1.5), and the change of velocity with respect to the standard deviation were used to remove invalid vectors and to interpolate between them. After the final cross-correlation, with an interrogation region of 32 × 32 pixels with 50 % overlap, which corresponds to a size of 1.58 × 1.58 mm, the data were subjected to a 3 × 3 Gaussian smoothing operation. In the case of SPIV, the two velocity fields extracted from the two individual cameras were combined to yield three-component velocity vectors. On average about 92 % valid vectors were obtained in the particle-seeded field of view. It has to be borne in mind that,

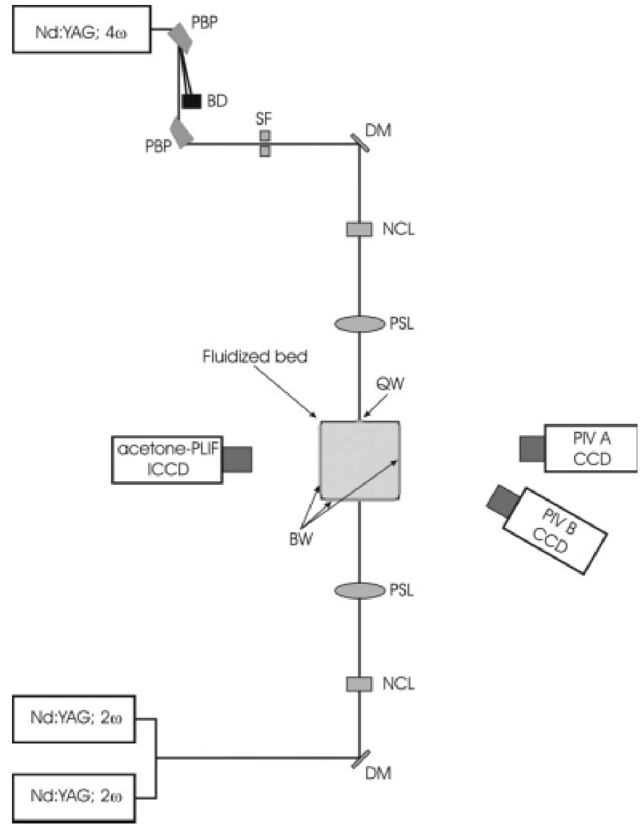

Figure 3. Schematic setup for the application of simultaneous acetone PLIF and PIV in the fluidized bed.

For 2D-PIV only camera PIV A was used; for SPIV both cameras (PIV A and PIV B) were used. Description of optical components: P BP Pellin-Broca prism, SF -spatial filter, BD -beam dump, DM -dichroic mirror, NCL -negative cylindrical lens, PSL -positive spherical lens, QW -quartz window, BW -B270 (Schott AG, Germany) window.

upon eruption of the bubbles, part of the laser sheet becomes blocked, and, thus, no vectors can be processed beyond this horizontal point due to lack of illumination of the tracer particles. Of course, this is also the case for acetone-PLIF which is described next.

2. Acetone-PLIF. Planar laser-induced fluorescence of acetone (C_3H_6O) was studied in the freeboard of the fluidized bed. The diagnostic system consisted of a frequency quadrupled Nd:YAG laser (Continuum Surelite II) for the excitation of acetone at 266 nm and a high-resolution ICCD camera (Lavision Nanostar, 1280 × 1024 pixels, Germany), which was used to image the acetone-PLIF signals. The images were digitised with 16-bit precision, with a true 12-bit dynamic range. The experimental set-up is as illustrated in Figure 3. The PIV laser sheets were overlapped with the acetone-PLIF sheets in a counter-propagating configuration as shown in Figure 3. The acetone fluorescence signal is smaller by several orders of magnitude compared to the Mie-scattering signal from both the particles seeded to the gas-flow passing through the fluidized bed, and the sand thrown into the freeboard upon bubble eruption. It, is, therefore, crucial to suppress any laser radiation at 1,064 nm and 532 nm, which passes through the frequency quadrupling unit of the laser. This was achieved using two Pellin-Broca prisms set in series. Pellin-Broca prisms offer the advantage of reflecting light of different wavelengths at significantly different angles, which in turn permits the separation of the laser radiation of interest (266 nm) from the residual laser radiation at 1,064 nm and 532 nm with high efficiency. The use of Pellin-Broca prisms leads to far superior rejection ratios of 532 nm and 1,064 nm laser light compared to the use of dichroic mirrors, as commonly applied for this purpose.

The UV-laser beam (pulse energy: 60 mJ) was spatially filtered and expanded into a collimated sheet with a height of 60 mm and a thickness of 120 μm, using a cylindrical planoconvex lens with focal length f = −25 mm, and a spherical lens with focal length f = +500 mm. A region 100 mm wide and 55 mm high was imaged using the ICCD, and PLIF images were recorded at 5 Hz repetition rate. The camera was fitted with a f/1.2 camera lens (Nikkor) equipped with two WG 305 filters and one BG 3 filter (Comar). It is crucial to prevent any Mie-scattering signal at 266 nm from being recorded by the ICCD camera as this could erroneously be interpreted as an acetone PLIF signal. Therefore, two measures have been applied in this study to eliminate this: (1) The use of two WG 305 filters rejects radiation at $\lambda = 266$ nm by a factor larger than 10^{10} (Schott, Germany), and (2) the window, through which the acetone-fluorescence is imaged (B270, Schott AG, Germany), reduces the light at $\lambda = 266$ nm by another factor of 10^5. These arrangements also reduce the risk of over-exposing the camera intensifier, and causing irreversible damage. The BG 3 filter was employed to suppress radiation of greater than $\lambda = 470$ nm from reaching the detection device. The recorded acetone PLIF images were first corrected for background and laser sheet inhomogeneities. Subsequently, noise was reduced by applying a median filter. Initial experiments did not result in a sufficient signal-to-noise ratio in the acetone-PLIF images. However, several modifications[19] resulted in s/n-ratios of about 80, which was regarded as sufficient for the analysis of the turbulent phenomena in the freeboard of the fluidized bed.

Sand from the fluidized bed entraining the freeboard upon bubble eruption will lead to Mie signal detected on the PIV cameras, and, thus, erroneous velocity measurements, because in contrast to the PIV seed particles the much larger bed particles do not follow the flow. However, these erroneous velocity vectors are easily detected and eliminated along the PIV-vector post processing. In this step velocity vectors which deviate more than one standard deviation in magnitude are removed. As a result of this no vectors were obtained from regions which were clearly identified as bubbles from the acetone PLIF-image, because the likelihood for large bed particles to be entrained into the flow is largest in these areas.

Triggering

All laser and cameras were triggered from a programmable time unit, controlled by the Davis software (Davis 6.2, Lavision, Germany). The Davis software, in turn was triggered from a 40 MHz arbitrary waveform generator (TGA1242, TTi, U.K.).

Results

In the following, simultaneous PIV (2D-PIV and SPIV) and acetone-PLIF measurements of the eruption of a single bubble and of a continuous stream of bubbles are presented. In addition, to shed further light on the dynamics of bubble eruption, PIV images of the velocity of the particles in the dome are presented. These images, acquired in a 2-D fluidized bed of height, width and transverse thickness of 500 × 194 × 10 mm, respectively, have been previously reported by Müller et al.[6]

Owing to the deposition of PIV tracer particles on to the windows of the fluidized bed, the transmission of the windows changed by about 15 % within a typical data acquisition time of about 3 min. Consequently, the acetone concentrations reported in this article are qualitative. Thus, in the following results, for each acetone-PLIF image in a figure, the acetone-PLIF images were normalized by a value C. For each sub-image in a figure, the probability density function (pdf) of the signal intensity was calculated from images which had been corrected for background and beam-profile. For each image, the 97.5 % maximum concentration, C_{local}, was determined from the pdfs. The value of C was chosen to be the maximum of all values of C_{local}.

Single bubble injected into a bed of Geldart Group B particles

These measurements have been reported previously.[19] More detailed information on the dynamics of a bubble eruption event are shown in Figures 6 and 7 based on acetone-PLIF measurements at 5 Hz. Thus, the time elapsed between two successive images shown in Figures 4 and 6 is 0.5 s and 0.2 s, respectively. The features seen in Figures 4–7 will be described shortly, but first it should be noted that the simultaneous PLIF and SPIV measurements shown were acquired using a ''side setup'' of the cameras, i.e., the cameras were shifted toward one side of the bed, so that the field of view extended to one wall. A ''central setup'' of the cameras has been also applied and is presented for the case of the eruption of a continuous stream of bubbles. It was found that the eruption profiles are fairly symmetric. Thus, imaging mainly one side of the eruption events did not result in any loss of information. However, the side setup can be beneficial, as the entire flow field at one side of the axis of symmetry is imaged. It should be noted that as the PIV seeding particles reduce the visibility through the glass windows, the s/n-ratio of the simultaneous PIV and acetone-PLIF measurements is reduced compared with pure acetone-PLIF measurements. Therefore, more detailed structures can be observed in the pure acetone-PLIF measurements. However, the s/n-ratio achieved in the simultaneous PIV and acetone-PLIF is still very good, so that both the velocity of the gas and the presence of a ''diffusive-tracer'' can be followed simultaneously. However, as noted previously[19] it was necessary to apply several optimization techniques to obtain such a high (s/n)-ratio.

To link the measurements of the velocity of the gas phase made here, with the velocity of the particles at a rising and collapsing dome, PIV measurements of the velocity of the particles in a 2-D bed of width, height and transverse length

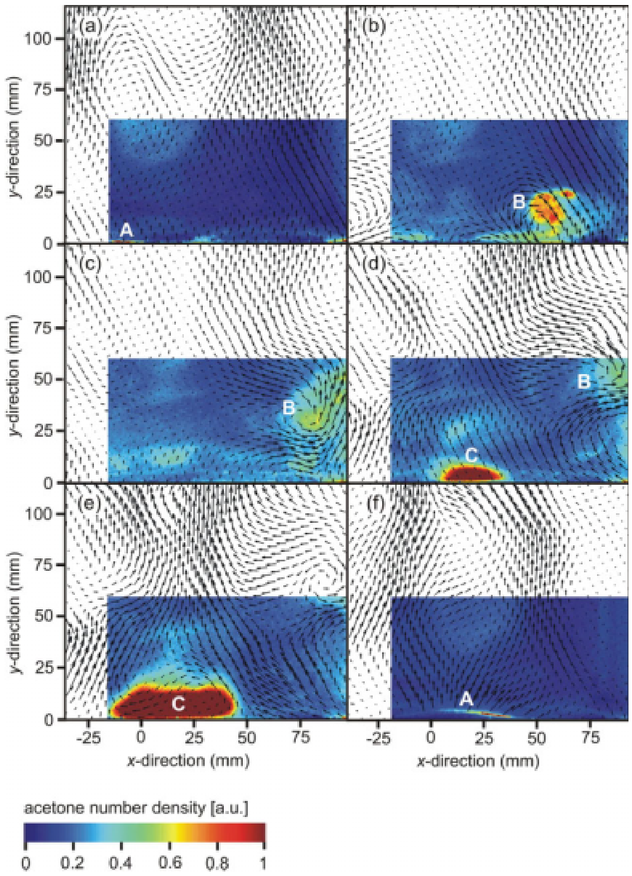

Figure 4. Simultaneous acetone-PLIF and stereoscopic PIV images of a single bubble erupting, D_e ∼45 mm mm, at the top of an incipiently fluidized bed. The time between two successive images is 0.5 s.

In Figure 4f a single frame of a separate bubble eruption event is shown. The vectors indicate the flow profile of the gas, whereas the color represents the acetone PLIF signal. Figures 4 and 5 show simultaneous SPIV and acetone-PLIF measurements of the eruption of a single bubble, injected into a bed of 150–250 μm glass spheres. Only one bubble eruption event is shown in Figures 4 and 5. The diameter of the bubble was D_e ∼45 mm. The maximum recording speed of the PIV-ICCD cameras was limited to 2 Hz. Consequently, the frame rate of the simultaneous SPIV and PLIF measurements was also limited to 2 Hz. For the acquisition of only acetone-PLIF measurements a higher frame rate, i.e., 5 Hz, was possible. [Color figure can be viewed in the online issue, which is available at www.interscience.wiley.com.]

of 500 × 194 × 10 mm, reported by Müller et al.[6] are shown in Figure 8. Of course, as the PIV measurements of the particle velocity were made in a 2-D bed, whereas the PIV measurements of the velocity of the gas phase were made in a 3-D bed, only qualitative links can be made. From the acetone-PLIF and PIV measurements shown in Figures 4–7, and the results in Figure 8, it can be seen that the eruption of a single bubble injected into an incipiently fluidized bed occurs in the following steps:

- The bubble, injected into the incipiently fluidized bed, forms a dome as it reaches the top surface of the fluidized bed, as seen in Figures 6a, labeled A, and 4a. It should be noted that the dome is just entering the field of view in Figure 4a. A better example of the formation of the dome is given in Figure 4f, which shows, however, a separate bubble eruption event. In the vicinity of the dome, the gas moves upward, similar to the motion of particles at a rising dome, as can be observed in Figure 8a.
- Release of a small pocket of acetone at the center of the dome, as seen in Figure 6b and is labeled "B". Solimene et al.[1] refer to this pocket as "nose pocket". However, in Hartung et al.[19] it was shown that the formation of a nose pocket is not the only possible eruption profile.
- In Figures 6b and 4b acetone also becomes visible at the outer margins of the dome. This is labeled C in Figure 6b. During this time the position of the "nose pocket" does not vary significantly. Some acetone of the "nose pocket" diffuses to the surroundings, leading to a smaller acetone signal, labeled B in Figure 6c. As observed in Hartung

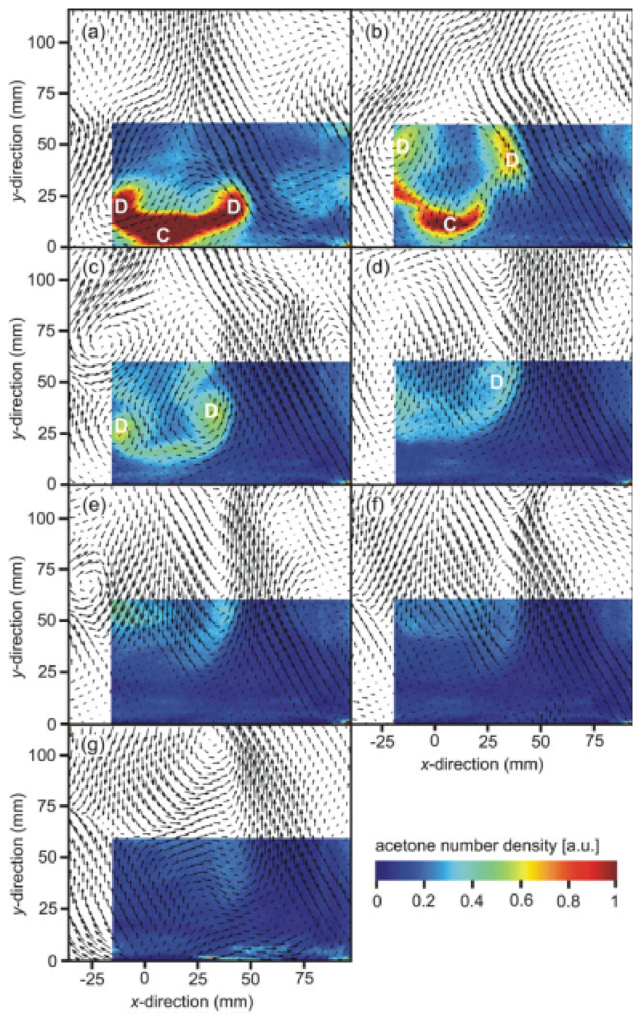

Figure 5. Simultaneous acetone-PLIF and stereoscopic PIV images of a single bubble erupting, D_e ∼45 mm mm at the top of an incipiently fluidized bed.

The time between two successive images is 1.0 s. The vectors indicate the flow profile of the gas, whereas the color represents the acetone PLIF signal. [Color figure can be viewed in the online issue, which is available at www.interscience.wiley.com.]

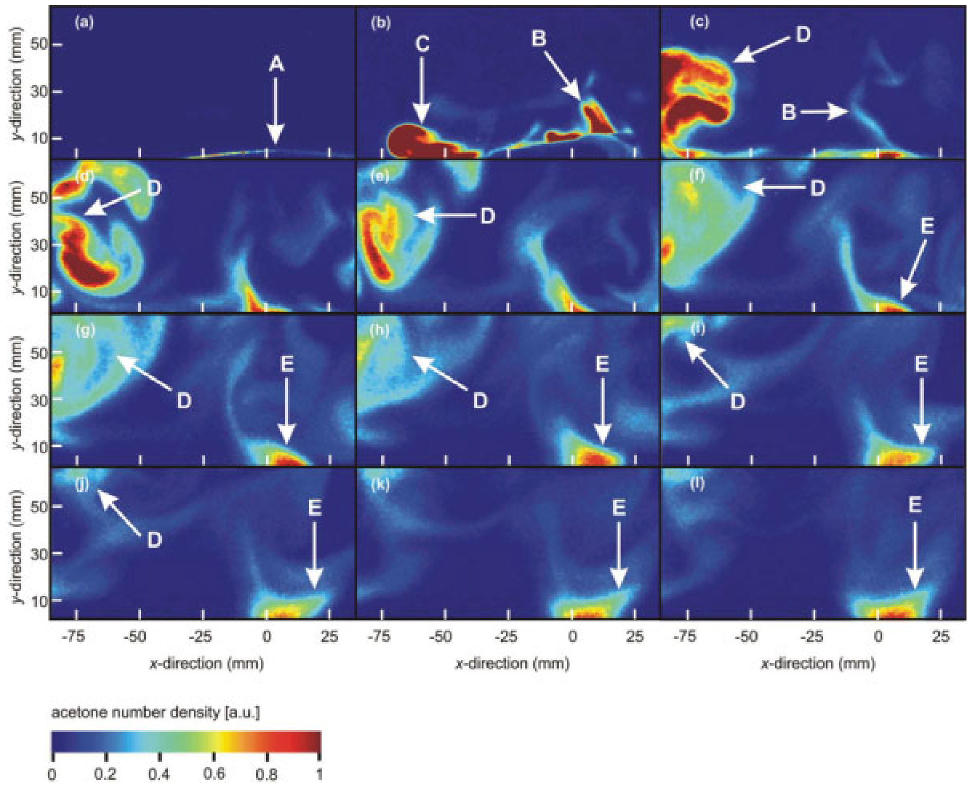

Figure 6. PLIF images of a single bubble erupting, D_e ~45 mm at the top of an incipiently fluidized bed.

The time between two successive images is 0.2 s. The higher frame rate is possible as only acetone-PLIF measurements were acquired.[19] Features labeled A-E are discussed in the text. [Color figure can be viewed in the online issue, which is available at www.interscience.wiley.com.]

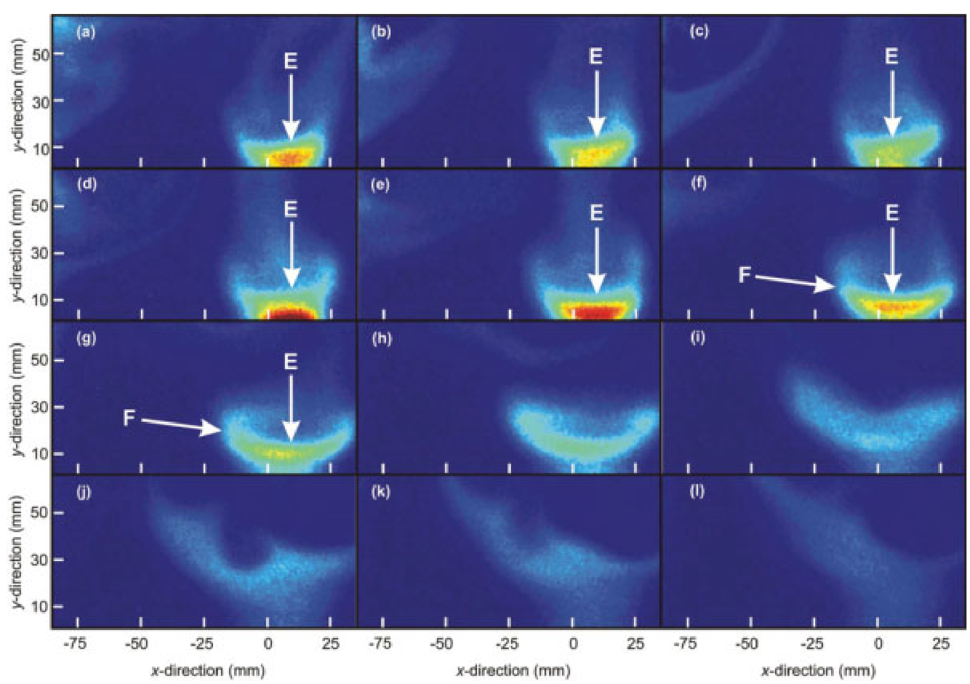

Figure 7. PLIF images following the bubble eruption shown in Figure 6. The time between two successive images is 0.4 s.

The higher frame rate is possible as only acetone-PLIF measurements were acquired.[19] [Color figure can be viewed in the online issue, which is available at www.interscience.wiley.com.]

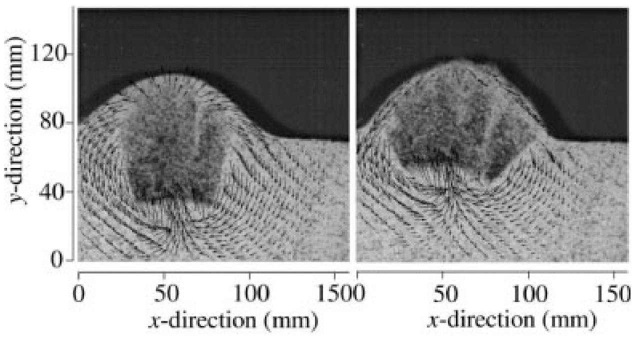

Figure 8. PIV images of the particle velocity around an erupting bubble.

The measurements were taken in a 2-D bed, and are reported by Müller et al.[6]: (a) rising dome, and (b) collapsing dome.

et al.[19] the nose pocket does not seem to move upward but moves indeed downward. This is caused by a high downward velocity of the surrounding gas toward the region where the dome had previously been. The mainly downward motion of gas at the center of the bed, i.e., for y ~20 mm is shown in Figure 4b. This velocity profile is very similar to the velocity of particles in a collapsing dome, which can be observed in Figure 8b.

• The acetone which was released at the margins of the collapsed dome moves toward the walls and exhibits a fairly complex structure. A strong horizontal motion close to the surface of the fluidized bed is shown in Figures 4b,c and 6b,d, labeled "D". A vertical cross-section of the toroidal vortex has the appearance of two "separate" vortices rings. These rings, rotating in opposite directions, i.e., clockwise at the left wall, and counterclockwise at the right wall. This is labeled B in Figure 4b. As Figures 4–7 use a side setup of the cameras, only one "vortex ring" is shown, i.e., the right one. The anticlockwise rotation is, however, clearly observable in Figure 4b and c. Confirmation of the clockwise rotation of the left part of the toroidal vortex is deferred until the images of the eruption of a continuous stream of bubbles are presented. These images were also acquired using a central setup of the cameras, thus, imaging the left and right part of the toroidal vortex, but not events at the walls of the bed.

• After some motion in the horizontal direction, i.e., toward the walls, the vortex is carried upward by the main flow field of the fluidized bed, as seen in Figures 4b–d labeled "B", and 6c–e, labeled "D". Due to the rotation and the rise of the vortex, acetone is, subsequently, shed from the initially confined region of acetone, leading to a more even distribution of acetone along the bed. However, almost no acetone can be found in the center of the freeboard.

• Just as the vortex rises close to the wall and sheds small pockets of acetone, a new region of acetone forms at the surface of the bed right at the position where the bubble originally erupted, labeled "E" in Figures 6f–l, and labeled "C" in Figure 4d and e. From this newly formed layer of acetone some acetone is initially released convectively and diffusively in the vertical direction. From Figure 4c and d it can be seen that the velocity profile at the center of the fluidized bed has been reversed, and the gas velocity is now directed upward. However, quite surprisingly, the vertical motion of the acetone is quite limited and restricted to only the first few frames after formation of the acetone layer at the surface, i.e., Figure 6c–e. From Figures 4d–e and 6g, the acetone released at the top of the bed has the shape of a thin layer, where most of the acetone, however, sheds away at the outer margins, forming two vortex rings rotating in opposite directions. This can be seen clearly from the simultaneous PIV and acetone-PLIF measurements, i.e., Figures 6e and 5a and b. As observed in Figures 6a and 5a and b, the left part of the vortex is rotating clockwise, whereas the right one is rotating in the opposite direction. This rotation results in a downward velocity at the center of the freeboard. Thus, the direction of the flow at the center of the freeboard, just above the surface of the bed, has reversed again. Consequently, the center of the freeboard contains only a little acetone and most of the acetone seems to be released along a concave upward curve.[19] The width and the thickness of the acetone layer is, initially, 50 mm and 10 mm, respectively. The formation of several vortices directly at the top of the bed can be seen in the following frames, i.e., Figures 5a–d, and 7a–c. The vortices are carried upward by the main gas-flow in the freeboard, become large in the process and subsequently lose their turbulent energy.

• Only after a significant amount of time, ~3.5 s, does the layer of acetone, formed at the top of the bed, detach from the top surface of the fluidized bed, and is carried into the freeboard where it finally mixes with the surrounding fluid, leading to a dispersion of the acetone signal. As the layer of acetone is detaching from the surface of the bed, the flow direction at the center of the bed just above the surface has been reversing for the last time. As seen in Figure 7e and g the direction of the flow is now upward. The release of acetone subsequent to a bubble eruption took in total ~4.5 s.

A comment regarding the velocity of the bubbles and the influence of the wake of the bubble on acetone mixing needs to be made at this point. In this study the bubble size was typically $D_e = 30 - 50$ mm, giving a ratio U_{mf}/U_b of ~1/14 – 1/18. As U_{mf}/U_b exceeds 1/10, this would indicate that the bubbles were "fast" and, consequently, that the cloud of the released bubbles was very thin.[20] Thus, only little gas exchange between the bubble and the bulk emulsion phase would be expected. However, as Rowe[23] and Collin[22] showed, respectively, experimentally and theoretically, this is probably not true for nonspherical bubbles, i.e., bubbles with a wake. Ultra-fast MR measurements confirm that bubbles are not spherical in the systems studied here.[21] Therefore, gas exchange between the gas phase in the bubble and emulsion phase would be expected. Acetone, which has been exchanged with emulsion phase would percolate through the bed with U_{mf}/ϵ_{mf}.[19] This phenomenon cannot be avoided, unless maybe very fine particles are used. However, the gas exchange between the bubble and the emulsion phase does not affect any conclusions drawn in this study. The information derived from the acetone PLIF measurements is mainly used at the instance of the eruption of the bubble. The release of acetone into the freeboard after the eruption of bubble does not affect any of these conclusions.

An interesting point is the decay of the bubble-induced turbulent energy of the vortices in the freeboard, shown in

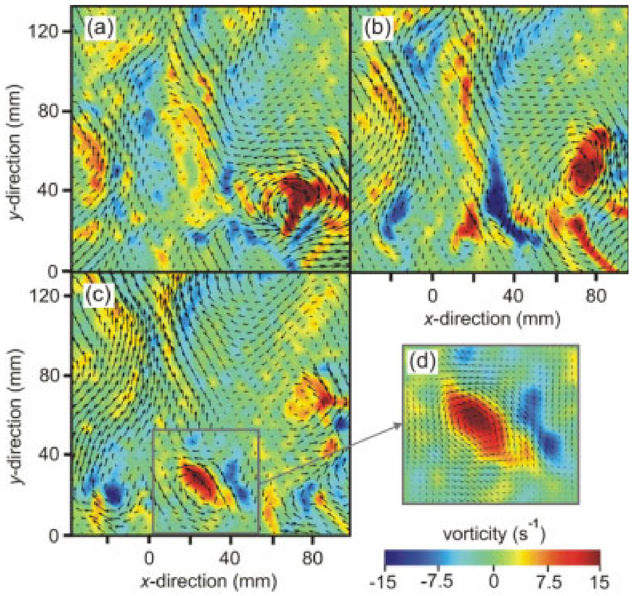

Figure 9. SPIV images where the vectors indicate the direction of the in-plane velocities, and the color represents the vorticity showing the transport and decay of the vortex formed upon collapse of the dome.

[Color figure can be viewed in the online issue, which is available at www.interscience.wiley.com.]

Figures 9 and 10. In Figures 9 and 10, the vectors indicate the direction of the velocity, whereas the color indicates the vorticity. Figure 9 shows the decay of the vorticity of a vortex formed upon the collapse of the dome. The vortex was first transported horizontally toward the walls. Within 1.5 s, the time elapsed between Figure 9a and c, the vorticity decreases from $\sim$15 s^{-1} to $\sim$2s^{-1}. In Figure 9c the shedding of two vortex rings from the acetone layer subsequently formed at the top of the bed is observed. As noted earlier, rotating in opposite directions. For clarity only every 6th vector is plotted in Figure 9. However, to give the reader a better idea of the detailed nature of the acquired SPIV measurements, all velocity vectors in a single vortex are plotted (Figure 9d). Figure 10 shows the decay of the vorticity of similar vortices as those shown in Figure 9c, i.e., vortices which were shed from the thin acetone layer formed at the top surface of the bed after the eruption of a bubble. From Figure 10 the decay of the vortex within 2 s can be clearly observed. The decrease in vorticity is accompanied by an enlargement of the vortex structure.

As SPIV measurements have been performed, the out-of plane component of the gas velocity, V_z, was also measured. A typical example of V_z is shown in Figure 11; the vectors indicate the in-plane flow direction, whereas the color gives the out-of-plane velocity component V_z. For example, in Figure 11b a clockwise rotating vortex can be seen. It is interesting that the out-of-plane component is by no means negligible. The maximum absolute values of V_x, V_y and V_z are 54 mms^{-1}, 87 mms^{-1}, and 61 mms^{-1}, respectively; their means are 6 mms^{-1}, 0.3 mm s^{-1}, and 6 mms^{-1}, respectively. Thus, Vz is of similar magnitude to the in-plane velocity components. The significance of the out-of-plane component is also shown in Figure 12, from which it can be seen that there is a considerable deviation around the mean, albeit that the maximum of the pdf is at 0.

Continuous stream of bubbles released in a bed of Geldart Group B particles

Figures 13 and 14 show simultaneous PIV and acetone-PLIF measurements of the eruption of a stream of bubbles continuously formed at the central orifice at the distributor. The bed was held at minimum fluidization and the flow rate through the 10 mm central orifice was 50 cc/s, i.e., the orifice velocity, U_O = 0.63 m/s. Both the ''central set-up'' and ''side setup'' of the ICCD cameras were used and are shown in Figures 13 and 14, respectively. For the central setup, 2D-PIV was applied, as a larger field of view can be achieved. From the results using the central setup it can be seen that the eruption profiles are fairly symmetric. Thus, imaging mainly one side of the eruption events did not cause any loss of information. From Figures 13 and 14, the following

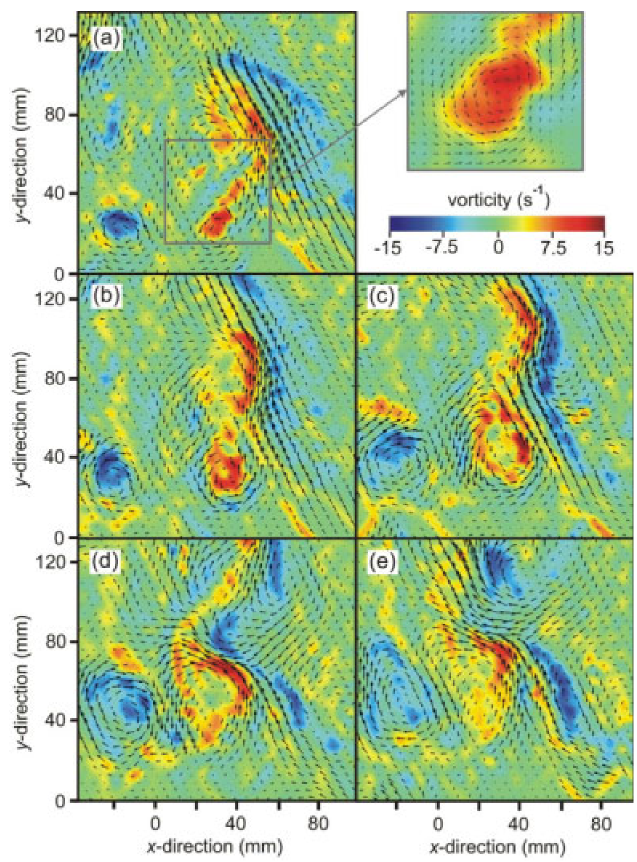

Figure 10. SPIV images where the vectors indicate the direction of the in-plane velocities, and the color represents the vorticity showing the transport and decay of the vortex shedding from the acetone layer formed at the bed's surface after the eruption of a bubble (time spacing: 0.5 s).

[Color figure can be viewed in the online issue, which is available at www.interscience.wiley.com.]

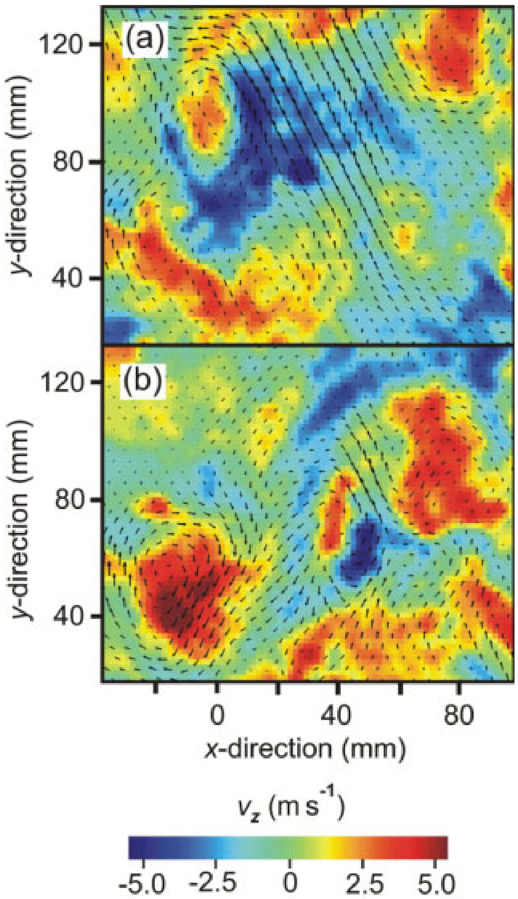

Figure 11. Typical example of a SPIV-only measurement.

The vectors indicate the in-plane flow direction, whereas the color gives the out-of-plane velocity component, V_z. [Color figure can be viewed in the online issue, which is available at www.interscience.wiley.com.]

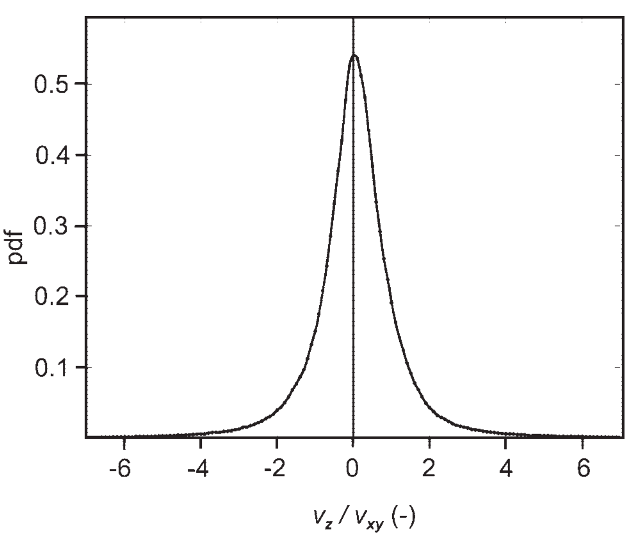

Figure 12. Probability distribution of the ratio of $V_z/\sqrt{V_x^2+V_y^2}$.

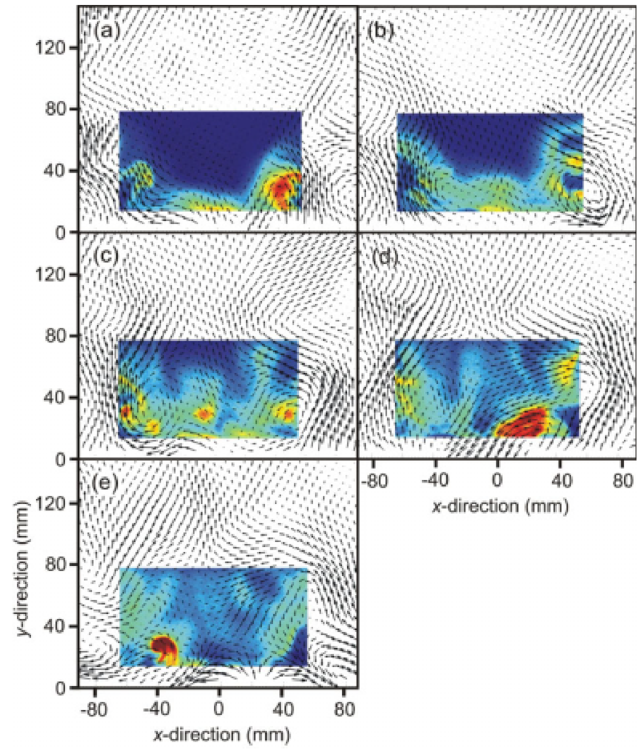

Figure 13. Simultaneous 2D-PIV (vectors), and PLIF (color) images acquired at 2 Hz showing the bubble eruption pattern of a continuous bubble stream.

The flow rate of the stream of bubbles was 50 cc/s, corresponding to an orifice velocity of U_O = 0.63 m/s (time spacing: 0.5 s). [Color figure can be viewed in the online issue, which is available at www.interscience.wiley.com.]

phenomena during the eruption of a continuous stream of bubbles can be observed:

- Similar to the results from the experiments involving the single injection of bubbles, most of the acetone of the erupting bubble is released at the outer margins of the formed dome.
- Upon collapse of the dome, a toroidal vortex forms, which is carried horizontally just above the surface of the fluidized bed toward the walls. In a vertical cross-section this toroidal vortex appears as two separate vortex rings, rotating in opposite directions, i.e., the left one rotates clockwise, and the right one counterclockwise, as seen in Figure 13c. These directions of rotation have been induced by a downward motion of the gas in the freeboard at the center of the fluidized bed, as seen in Figure 14c.
- Sometimes the formation of a small nose pocket can be observed, e.g., in Figure 14a. As can be seen in Figure 14a the nose pocket does not move upward, but rather moves downward, due to the velocity profile of the gas, which is downward upon dome collapse.
- In the vicinity of the walls the vortex is carried upward owing to the main gas flow in the freeboard. During this upward motion, surrounding gas is entrained in the vortices, and little pockets of acetone shed away leading to a decrease in vorticity and acetone signal, e.g., see Figure 14c–e.

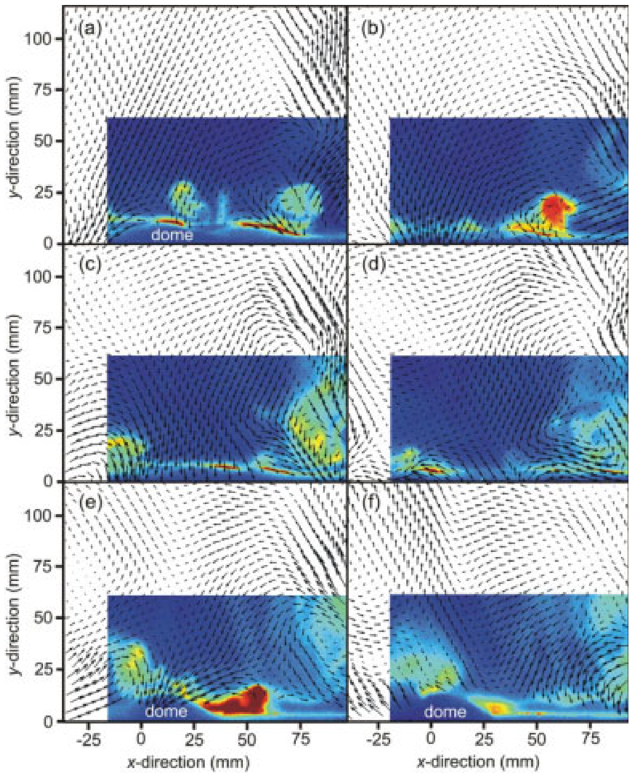

Figure 14. Simultaneous SPIV (vector) and PLIF (color) images acquired at 2 Hz showing the bubble eruption pattern of a continuous bubble stream.

The flow rate of the stream of bubbles was 50 cc/s, corresponding to an orifice velocity of $U_O = 0.63$ m/s (time spacing: 0.5 s). [Color figure can be viewed in the online issue, which is available at www.interscience.wiley.com.]

- Most of the acetone signal is usually observed at the position where the dome forms and close to the surface of the bed. However, close to the walls, directly above the surface of the fluidized bed very little acetone can be found. Here, mainly acetone free gas is released into the freeboard.

For measurements both of single bubbles and of a continuous stream of bubbles, it was observed, in agreement with Hartung et al.[19] that upon formation of the dome, acetone can escape in different ways, the main ones being: (1) formation of a ''nose pocket'' at the center of the dome, (2) release of acetone along the entire surface of the dome, or (3) release of acetone predominantly at the margins of the dome without the formation of a ''nose-pocket''. The simultaneous SPIV and acetone-PLIF measurements in this work showing the different eruption profiles described previously, are shown in Figure 15 for a continuous stream of bubbles, and confirm this observation.

It should be noted that attempts were made to use smaller particles, i.e., 59 – 150 μm glass ballotini, which fall in Geldart's group A. The acquisition of PIV measurements was not problematical and will be reported elsewhere. However, acetone PLIF measurements were not possible. An important requirement for acetone PLIF to work is that the acetone released by an erupting bubble is removed from the fluidized bed via the main flow. In a bed of Geldart's group A particles, the minimum fluidization velocity was very low; thus, acetone was removed only very slowly from the freeboard, resulting in a very quick saturation of the acetone signal in the freeboard.

Figure 16 shows time averaged velocity and acetone profiles. The averaging time was ~30 s. In Figure 16a and b, the vectors indicate the direction of the flow, whereas the color represents, respectively, the magnitude of the velocity and the acetone signal.

A central setup has been used in Figure 16a and b. A side setup is given in Hartung et al.[19] In agreement with,[19] the acetone release is axi-symmetric (Figure 16b). The acetone profile follows roughly along a concave curve upward and toward the walls, with almost no acetone being present in the center of the bed. A schematic sketch is given in Figure 16c. The time-averaged velocity profiles in Figure 16 explain such behavior. Figure 16a demonstrates that in the center of the fluidized bed, the time averaged velocity is downward, whereas the velocity is upward at the walls only. This results in a strong horizontal motion toward the walls in the vicinity of the surface of the fluidized bed. The effect of increasing volumetric flow rate is shown in Figure 17. As expected, an increase in volumetric flow rate through the central orifice results in an increase in upward and downward velocities near the walls and the center of the freeboard, respectively.

Discussion

PIV results, giving both the velocity of the *particles* in a forming and collapsing dome and of the *gas* in the freeboard, together with simultaneous acetone-PLIF

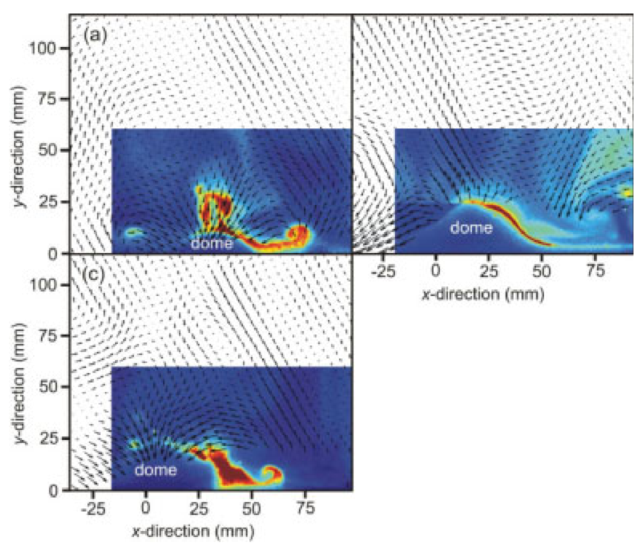

Figure 15. Simultaneous SPIV and PLIF images showing different eruption profiles: (a) formation of a nose pocket, (b) release of acetone along the entire surface of the dome, and (c) release of acetone predominantly at the margin of the dome without the formation of a "nose-pocket".

[Color figure can be viewed in the online issue, which is available at www.interscience.wiley.com.]

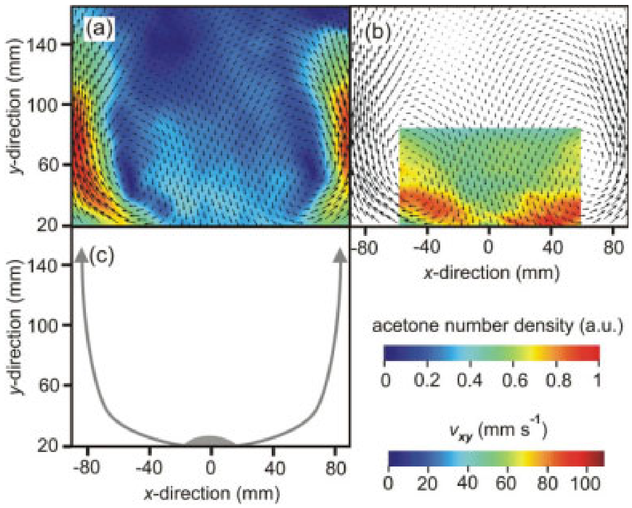

Figure 16. Time-averaged acetone signal for a continuous stream of bubbles.

In (a) the vectors indicate the direction of the flow, whereas the color represents the magnitude of the velocity, and in (b) the vectors give the direction of the flow, whereas the color represents the acetone PLIF signal. The flow rate through the orifice was 71 cc/s, corresponding to an orifice velocity of $U_O = 0.90$ m/s. Vectors indicate the direction of the time averaged in-plane velocities: (a) color represents the magnitude of the time averaged in-plane velocity, (b) color represents time-averaged acetone PLIF signal, and (c) schematic of the time-averaged acetone release. [Color figure can be viewed in the online issue, which is available at www.interscience.wiley.com.]

measurements has helped to shed light on the rather complex mechanisms occurring during the eruption of a bubble. Solimene et al.[1] applied acetone-PLIF and, separately, planar laser sheet scattering.[3] Despite providing very important and novel insights into the phenomenon of bubble eruption, their study had three disadvantages compared with the techniques applied here. First, the planar laser sheet scattering only provided information about a nondiffusive tracer during the bubble eruption event and not thereafter. Second, it is rather a technique for flow visualization, and does not provide quantitative measurement of the velocity field. Third, planar laser sheet scattering and acetone PLIF data were not acquired at the same time.

The results in Figures 4–7 from acetone-PLIF measurements of an erupting bubble, are in good agreement with the observations of Solimene et al.[1] Thus, most of the acetone escapes at the outer margins of the dome upon its collapse. PIV images also confirmed Solimene et al.'s[1] observations, that acetone, originally present in the erupting bubble, mainly escapes toward the walls. This is followed by the formation of a thin layer of acetone at the top of the fluidized bed. The thickness of the layer is ~10 mm, and its width is ~30 – 40 mm, rather smaller than the bubble diameter. The thickness of the acetone layer decreases with time. Using SPIV, the continuous shedding of the vortices from that layer of acetone was observed. Due to the diffusion of acetone, it is more difficult to observe the shedding of acetone in the PLIF measurements. Hartung et al.[19] proposed that the release of acetone at the top of the bed is caused by gas exchange between the bubble and the emulsion phase, as the bubbles studied have probably a wake angle of ~120°. The potential flow calculations of Collins[22] and experimental observations of Rowe[23] using NO_2 in a 2-D bed confirmed that theory. Furthermore, the time until the acetone layer is observed is in close agreement with the time required for the gas to percolate through the fluidized bed, t_r, i.e., $t_r = H_{mf}\,\varepsilon_{mf}/U_{mf}$, where H_{mf} and ε_{mf} are the height and the voidage of the bed at incipient fluidization.

Solimene et al.[1] observed the formation of a so-called nose-pocket and attributed its formation to some through flow of gas from the erupting bubble through the dome. As shown by Müller et al.[6] the dome thickness in 2-D beds is not even over its angle of eruption. The dome is often thinnest around its center. This explains why, often, gas from the bubble escapes at the center of the dome. However, due to the local heterogeneity of the dome thickness it is also possible that the dome breaks first at a location different from the center, which would explain the other eruption patterns observed here. It is assumed that the dome thickness becomes more complicated in a 3-D system, but no experimental measurements are available so far.

PIV measurements of the velocity of both the gas and the bed particles (Figures 6 and 8) also support the model of Solimene et al.[1] that the collapse of the dome causes a change of momentum of the surrounding gas. Upon collapse of the dome, the surrounding gas moves toward the original center of the erupted bubble. This causes the remaining gas of the erupting bubble to be "squeezed"[1] toward the walls of the fluidized bed. The PIV data presented here confirms a strong horizontal velocity just above the surface of the fluidized bed, which would explain the formation and motion of the toroidal vortex toward the walls. However, it is not conclusively clear, either from our or Solimene et al.'s (2007) PLIF images at what stage acetone is "squeezed" from the dome. In other words, whether it occurs during bubble eruption or only after a bubble has collapsed. To answer that question, unequivocally higher

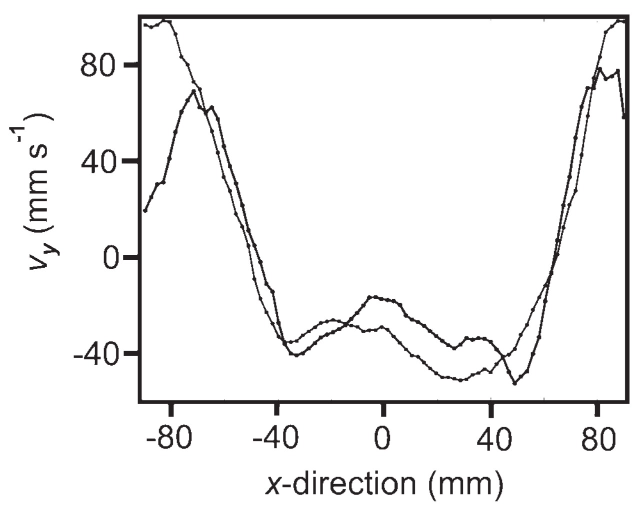

Figure 17. Variation of the time-averaged vertical velocity in the freeboard with flow rate through the central orifice.

The velocities are compared 30 mm above the surface of the bed: (--) Q = 50 cc/s, (--) Q = 85 cc/s.

frame rates are required which were, however, not possible with the equipment used here.

Comparing the velocity and acetone concentrations in Figures 13 and 14 confirms that the eruption of a continuous stream of bubbles occurs in an axi-symmetric fashion. There does not seem to be a qualitative difference between the eruption of a single bubble and that of a stream of bubbles.

The time-averaged velocity profiles, presented in Figure 16, show a gross circulation profile, with gas moving downward at the center of the fluidized bed and upward at the walls, with a strong horizontal component toward the walls at the vicinity of the bed's surface. This observation is in agreement with measurements of Duursma et al.[7] albeit made higher up the bed, i.e., 0.4 m above the defluidized bed surface. Time-averaged acetone-PLIF measurements, Figure 16, are in agreement with the velocity measurement, i.e., most of the acetone can be found along an upward curve as depicted schematically in Figure 16, with the majority being released at the outer margin of the dome. At the center of the bed only very little acetone can be found as the time-averaged velocity profile indicates downward gas motion, thus, allowing no convective acetone transport in the upward direction. In the vicinity of the walls, just above the bed's surface, acetone-free air is present, as the gas exchange between the bubble phase and the emulsion phase is limited to the thin cloud of the bubble.

Conclusions

Simultaneous PIV and acetone-PLIF measurements in the freeboard of a gas-fluidized bed are reported here for the first time. In addition, for the first time stereoscopic PIV has been applied in gas-fluidized beds, thus, providing measurements of the out-of-plane component of the velocity of the gas in the freeboard. The following conclusions can be drawn from this study:

- The observed profiles of bubble eruption follow generally the models proposed by Levy et al.[24,5] and Solimene et al.[1]
- In addition to the observations of Solimene et al.[1] different ways of acetone tracer release were observed upon the formation of the dome. This was attributed to the inhomogeneity of the thickness of the dome as observed in 2-D beds reported by Müller et al.[6]
- The out-of plane component is not negligible as it is often of the same order of magnitude as the in-plane velocity components.
- The bubble eruption profile of a stream of bubbles is qualitatively very similar to the eruption of single bubble.
- The time-averaged flow profiles show downward motion of the gas in the center of the fluidized bed and upward motion at the walls, with a strong horizontal component close to the surface of the fluidized bed.
- The vorticity of the vortices, shed from an acetone layer, which forms after the bubble eruption, decays quite rapidly, typically within 2 s.

Acknowledgements

We would like to thank F. Scheel and the DLR for the loan of the PIV seeder. We are also grateful to Dr. T. Nickels for help with the PIV software. This work was supported by grants from the EPSRC and grants from EU's Sixth Framework Programme INTELLECT D.M. contract (EU Project AST3-CT-2003-502961, Jan 01, 2004 -Dec 31, 2007). CRM acknowledges financial support from the Deutscher Akademischer Austauschdienst (DAAD) and Cambridge European Trust. GH is grateful to a case studentship from CMI (Cambridge-MIT Institute) and Intellect D.M. JH was supported by an Advanced Research Fellowship from the EPSRC (EP/C012399/1). CFK is thankful to the Leverhulme trust for personal sponsorship.

Literature Cited

1. Solimene R, Marzocchella A, Ragucci R, Salatino P. Laser diagnostics of hydrodynamics and gas-mixing induced by bubble bursting at the surface of gas-fluidized beds. *Chem Eng Sci*. 2007;62:94–108.
2. Hamdullahpur F, MacKay GDM. Two-phase flow behaviour in the freeboard of a gasfuidized bed. *AIChE J*. 1986;32:2047–2055.
3. Solimene R, Marzocchella A, Ragucci R, Salatino P. Flow structure and gas-mixing induced by bubble bursting at the surface of an incipiently gas-fluidized bed. *Ind Eng Chem Res*. 2004;43:5738–5753.
4. Zenz FA, Weil NA. A theoretical-empirical approach to the mechanism of particle entrainment from fluidized beds. *AIChE J*. 1958;4:472–479.
5. Yorquez-Ramirez MI, Duursma GR. Insights into the instantaneous freeboard flow above a bubbling fluidized bed. *Powder Technol*. 2001;116:76–84.
6. Müller CR, Davidson JF, Dennis JS, Hayhurst AN. A study of the motion and eruption of a bubble at the surface of a two-dimensional fluidized bed using particle image velocimetry (PIV). *Ind Eng Chem Res*. 2007;46:1642–1652.
7. Duursma GR, Glass DH, Rix SJL. Yorquez-Ramirez M.I. PIV investigations of flow structures in the fluidized bed freeboard region. *Powder Technol*. 2001;120:2–11.
8. Pemberton ST, Davidson JF. Elutriation from fluidized beds -1. Particle ejection from the dense phase into the freeboard. *Chem Eng Sci*. 1986;41:243–251.
9. Kehoe PWK. *The effect of particle size on slugging fluidized beds*. University of Cambridge, U.K; 1969. PhD disseration.
10. Thurber MC, Hanson RK. Pressure and composition dependences of acetone laser-induced fluorescence with excitation at 248, 266, and 308 nm. *Applied Physics B, lasers and optics*. 1999;69:229–240.
11. Hult J, Richter M, Nygren J, Aldén M, Hultqvist A, Christensen M, Johansson B. Application of a high-repetition-rate laser diagnostic system for single-cycle-resolved imaging in internal combustion engines. *Applied Optics*. 2002;41(24):5002–5014.
12. Su LK, Clemens NT. Planar measurements of the full three-dimensional scalar dissipation rate in gas-phase turbulent flows. *Exp Fluids*. 1999;27:507–521.
13. Patrie BJ, Seizman JM, Hanson RK. Instantaneous three-dimensional flow visualization by rapid acquisition of multiple planar flow images. *Optical Eng*. 1994;33:975–980.
14. Hinsch KD. 3-Dimensional particle velocimetry. *Meas Sci Technol*. 1995;6(6):742–753.
15. Mullin JA, Dahm WJA. Dual-plane stereo particle image velocimetry measurements of velocity gradient tensor fields in turbulent shear flow. I. Accuracy assessments. *Phys Fluids*. 2006;18(3):035101.
16. Mullin JA, Dahm WJA. Dual-plane stereo particle image velocimetry measurements of velocity gradient tensor fields in turbulent shear flow. II. Experimental results. *Phys Fluids*. 2006;18(3):035102.
17. Prasad AK. Particle image velocimetry. *Current Sci*. 2000;79(1):51–60.
18. Scarano F, Riethmuller ML. Iterative multigrid approach in PIV image processing with discrete window offset. *Exp Fluids*. 1999;26(12):513–523.
19. Hartung G, Müller CR, Hult J, Kaminski CF, Dennis JS. Laser diagnostic investigation of the bubble eruption patterns in the freeboard of fluidized beds. Part 1: Optimized acetone PLIF measurements. *Ind Eng Chem Res*. 2008;47:5686–5697.

20. Davidson JF, Harrison D. *Fluidized particles*. Cambridge University Press; 1963.
21. Müller CR, Holland DJ, Davidson JF, Dennis JS, Gladden LF, Hayhurst AN, Mantle MD, Sederman AJ. Rapid two-dimensional imaging of bubbles and slugs in a three-dimensional, gas-solid, two-phase flow system using ultrafast magnetic resonance. *Phys Rev E*. 2007;75:020302 (R).
22. R.Collins, An extension of Davidson's theory of bubbles in fluidized beds. *Chem Eng Sci*. 1965;20:747–755.
23. Rowe PN. Private communication. Atomic Energy Research Establishment, Harwell. The image is shown in ref. 20.
24. Levy EK, Caram HS, Dille JC, Edelstein S. Mechanism for solids ejection from gas-fluidized beds. *AIChE J*. 1983;29:383.
25. Anderson DJ, Greated CA, Jones JDC, Nimmo G, Wiseall S. Fibre optic PI studies in an industrial combustion. *Proceedings of the 8th International Symposium on Applications of Laser Techniques to Fluidmechanics*. 1996;18.4:86.
26. Yoon J-H, Lee S. Direct comparison of 2D PIV and stereoscopic PIV measurements. *Meas Sci Technol*. 2002;13:1631–1642.

Manuscript received Oct. 31, 2007, revision received Aug. 31, 2008, and final revision received Dec. 6, 2008.